

DIDA: Denoised Imitation Learning based on Domain Adaptation

Kaichen Huang^{*1,2} Hai-Hang Sun^{*1,2} Shenghua Wan^{1,2} Minghao Shao^{1,2} Shuai Feng³ Le Gan^{1,2}
De-Chuan Zhan^{1,2}

Abstract

Imitating skills from low-quality datasets, such as sub-optimal demonstrations and observations with distractors, is common in real-world applications. In this work, we focus on the problem of *Learning from Noisy Demonstrations* (LND), where the imitator is required to learn from data with noise that often occurs during the processes of data collection or transmission. Previous IL methods improve the robustness of learned policies by injecting an adversarially learned Gaussian noise into pure expert data or utilizing additional ranking information, but they may fail in the LND setting. To alleviate the above problems, we propose **Denoised Imitation learning based on Domain Adaptation (DIDA)**, which designs two discriminators to distinguish the noise level and expertise level of data, facilitating a feature encoder to learn task-related but domain-agnostic representations. Experiment results on MuJoCo demonstrate that DIDA can successfully handle challenging imitation tasks from demonstrations with various types of noise, outperforming most baseline methods.

1. Introduction

Imitation Learning (IL) (Schaal, 1999; Ross & Bagnell, 2010; Hussein et al., 2017; Osa et al., 2018; Zhang et al., 2023; Gandhi et al., 2023) has made rapid progress in many challenging fields including game playing (Haliem et al., 2021; Shi et al., 2023), financial trading (Peng & Lee, 2023) and robotics (Duan et al., 2023; Davis et al., 2023; Belkhale et al., 2023). In addition to the performance of a model, robustness and noise resilience are also important factors in IL algorithms designed for real-world problems. In this work, we focus on the problem of *Learning from Noisy Demonstrations* (LND), whose name has been proposed by (Tangkaratt et al., 2020). However, the specific problem setting in our work is quite different: the previous work learned from a mixture of expert and non-expert data, where the term “imperfect” is more appropriate than “noisy”; while we attempt to learn from expert data with various noise that

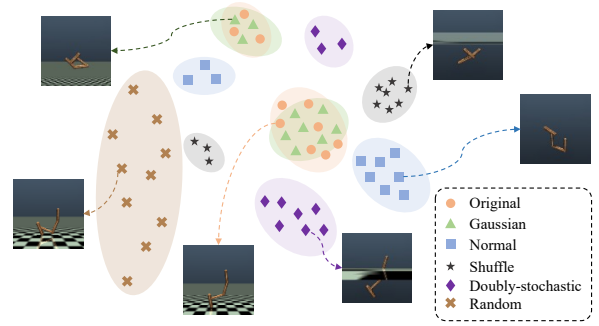


Figure 1. The **simplified** t-SNE (Van der Maaten & Hinton, 2008) plot of states in collected trajectories. We selected 10 data points of each class from the original plot (Figure 15) and displayed them using different colors and shapes. The arrows point to the rendered images using noisy underlying states, demonstrating the significant impact of noise on observations.

are common in the real world.

The environment in our world is not a perfect simulator. Human experts may make mistakes; information encounters all kinds of noise during its transmission through a medium; sensors can suddenly malfunction. Even when we possess a perfect expert, the produced demonstrations may also become noisy when they reach the agent. Noise is inevitable in the real world. Therefore, making agents (also called imitators) robust to noise is crucial to the applications of IL methods.

Previous robust IL methods (Laskey et al., 2017; Brown et al., 2020; Chen et al., 2021; Wang et al., 2022) generally improve the robustness of the learned policy by injecting non-expert data or adversarially learned Gaussian noise into pure expert data. Some of which use additional ranking information. However, in most real-world scenarios, noisy expert data is more accessible than pure expert data, thus the LND setting that we propose is more realistic. There also exist methods (Tangkaratt et al., 2020; Chen et al., 2023; Yuan et al., 2023) learning from noisy expert data, however, they can handle either small scales of noise or only a single type of noise.

To alleviate the above problems, we propose **Denoised**

Imitation learning based on **Domain Adaptation (DIDA)**, which jointly learns a noise discriminator, a policy discriminator, and a feature encoder to learn representations that are task-related but domain-agnostic. Empirically, we find that *DIDA can learn from fully noisy data without explicit knowledge of pure expert* and can solve a variety of noise, including additive noise and multiplicative noise.

Our main contributions are summarized as follows:

- 1) We formally define a variety of noise for IL, including additive and multiplicative noise, and we theoretically analyze the limitations of GAIL in solving LND problems.
- 2) We propose DIDA, a domain-adaptation-based Imitation Learning method, to imitate expert policy from noisy demonstrations in an adversarial manner, extracting domain-agnostic features and capturing the underlying expertise behind the noisy data.
- 3) Experiments on 10 distinctive tasks with various types of noise on MuJoCo show the desirable performance of DIDA on LND problems.

2. Related Work

Many previous works focus on robust IL methods: DART (Laskey et al., 2017) injects noise into the expert’s policy to reduce covariate shifts; RIL-Co (Tangkaratt et al., 2020) learns from a mixture of expert and non-expert demonstrations by co-pseudo-labeling; ARIL (Wang et al., 2022) designs an adversary to inject noise into real states, and jointly trains the agent’s and adversary’s policies; RIME (Chae et al., 2022) attempts to learn a robust policy by leveraging expert data from different MDPs. These methods require either expert policy or pure expert data; in contrast, *DIDA only relies on fully noisy data*. D-REX (Brown et al., 2020) and SSRR (Chen et al., 2021) use noisy policy to generate ranked trajectories and increase the robustness of the reward function respectively; other works (Burchfiel et al., 2016; Brown et al., 2019; Wu et al., 2019; Zhang et al., 2021) utilize ranking information among demonstrated trajectories by preference learning. Compared with the above methods, DIDA does not require additional ranking information, so it can work in situations where human ranking or querying is inaccessible.

DIDA adopts the framework of Adversarial Imitation Learning (AIL), where IL is interpreted as a divergence minimization problem (Ho & Ermon, 2016; Ghasemipour et al., 2020; Ke et al., 2021). Additionally, to obtain consistent representations, DIDA adopts the domain adversarial training paradigm, which has been involved in some IL methods (Stadie et al., 2017; Sharma et al., 2019; Liu et al., 2019; Cetin & Celiktutan, 2021). These methods treat imitation as a cross-domain problem and instruct the imitator to learn from expert demonstrations collected in a different domain.

Our DIDA is closely related to these works, but has the following differences: 1) DIDA utilizes domain adaptation to learn from completely noisy data, while other methods learn from pure expert data. 2) We design a *self-adaptive rate* and a *domain adversarial sampling (DAS)* method to facilitate DIDA training in a self-adaptive way. 3) Many previous works require a *random* dataset to help domain adaptation; we propose a new way to design such datasets that we call *anchor buffer*, and illustrate its effect.

3. Problem Setting

Suppose the expert buffer $\mathcal{B}_E = \{\tau_i^E\}_{i=1:T}$, where $\tau^E = \{(s_t, a_t)\}_{t=1}^H$. The noisy data can be generated by:

$$\tilde{s}_i = f_{\text{noise}}(s_i) = f_i(A_i s_i + B_i) \quad (1)$$

$$\tilde{\tau}_i = f_{\text{noise}}(\tau_i) = \{\tilde{s}_1, a_1, \dots, \tilde{s}_H, a_H\} \quad (2)$$

where $A \in \mathbb{R}^{n \times n}$, s and B are n -D vectors, $f(\cdot)$ is a transformation, which can be linear or nonlinear, and f_{noise} is the noise operator. Subscript i indicates that these components can be time-varying. We only consider the *linear time-invariant (LTI)* (Gu & Dao, 2023) noise on states: $\tilde{s}_i = f_{\text{noise}}(s_i) = A s_i + B$. We ignore the noise on actions because the states usually have much higher dimensions than actions and thus are easier and more likely to be affected by noise. Our work primarily addresses two common noise in the signal transmission theory:

Additive noise can be added to the signal (expert data) and we formalize it as **Gaussian** noise. We set A to be the identity matrix, and the elements of B are sampled from $\mathcal{N}(\mu, \sigma^2)$, where μ and σ denote the expectation and standard deviation.

Multiplicative noise is generally caused by imperfect channels and can be multiplied by the signal. Setting B as zero vector, different choices of A can lead to various noise:

1) **Normal**: Elements of A are sampled from $\mathcal{N}(0, 1)$. The resulting normal matrix multiplied by s is equivalent to applying a linear transformation on the state feature space.

2) **Doubly-stochastic**: We set A as a doubly-stochastic matrix, whose elements are all non-negative, and the sum of each row and column is equal to 1. Thus each element of \tilde{s} is the weighted sum of all n elements of s . The significance of studying *Doubly-stochastic* noise is that if we can solve it, then its subclasses (such as permutation matrices and transition matrices) are also solvable.

3) **Shuffle**: We set A as a permutation matrix, which is a special case of the doubly-stochastic matrix. *Shuffle* noise randomly permutes the dimensions of the state, which can simulate the disordered sensor data in reality.

In addition, we define the **combined** noise, i.e., we uniformly and randomly divide the expert dataset into four parts, add

the four noise defined above, and finally mix them up to form one dataset.

We show the simplified t-SNE plot corresponding to different noisy data in Figure 1, where the relative positions of different noise clusters in the figure reflect their properties. *Original* and *Random* are generated with the expert and random policies respectively and the other classes are obtained by adding different noise to *Original*. *Gaussian* surrounds *Original*; *Random* is the most dispersed; others have similar shapes to *Original*, but differ in position.

Definition of training data. Let $\tau^E = \{(s_t^E, a_t^E)\}_{t=1}^H$ and $\tau^I = \{(s_t, a_t)\}_{t=1}^H$ denote the expert and imitator trajectories sampled with the expert policy π_E and the imitator policy π respectively. We define the expert buffer $\mathcal{B}_E = \{\tau_i^E\}_{i=1}^T = \{(s_t^E, a_t^E)\}_{t=1}^{T \times H}$ ¹ and the imitator buffer $\mathcal{B}_I = \{\tau_i^I\}_{i=1}^T$ in the same way. Then we construct the noisy expert buffer $\tilde{\mathcal{B}}_E$:

$$\begin{aligned} \tilde{\mathcal{B}}_E &= f_{\text{noise}}(\mathcal{B}_E) = \{f_{\text{noise}}(\tau_i^E)\}_{i=1}^T \\ &= \{f_{\text{noise}}(s_t^E), a_t^E\}_{t=1}^{T \times H} \\ &= \{(As_t^E + B, a_t^E)\}_{t=1}^{T \times H} \end{aligned}$$

where noise operator f_{noise} is either a single LTI noise or a mixture of multiple LTI noise. As shown in Figure 2, by treating the expertise level and the noise level as the coordinate axes, we can place the datasets defined above into the four quadrants of the Cartesian coordinate system. For simplicity, we define the four quadrants of the coordinate axes as different domains \mathcal{D}^{EN} , \mathcal{D}^{RN} , \mathcal{D}^{RP} , and \mathcal{D}^{EP} , where (E, R, N, P) denote (**Expert**, **Random**, **Noisy**, **Pure**). Additionally, we define the expert domain \mathcal{D}^{E} as $\mathcal{D}^{\text{EN}} \cup \mathcal{D}^{\text{EP}}$, and define the random domain \mathcal{D}^{R} , the noisy domain \mathcal{D}^{N} , and the pure domain \mathcal{D}^{P} similarly.

Learning from noisy demonstrations (LND). Considering the Markov Decision Process (MDP) setting, we assume that the expert π_E and the imitator π share the same dynamics $\mathcal{M} = (\mathcal{S}, \mathcal{A}, \mathcal{P}, r, \gamma, p_0)$, where \mathcal{S} is the state space, \mathcal{A} is the action space, $\mathcal{P}: \mathcal{S} \times \mathcal{A} \rightarrow \mathcal{S}$ is the transition function, $r: \mathcal{S} \times \mathcal{A} \times \mathcal{S} \rightarrow \mathbb{R}$ is the reward function, $\gamma \in [0, 1)$ is the discount factor, and p_0 is the initial state distribution. According to Proposition 3.1 in (Ho & Ermon, 2016), the occupancy measure $\tilde{\rho}_e$ derived from the noisy expert buffer $\tilde{\mathcal{B}}_E$ refers to a unique corresponding noisy expert policy $\tilde{\pi}_E$, and the same is true for the anchor domain $(\tilde{\mathcal{B}}_A, \tilde{\rho}_A, \tilde{\pi}_A)$ that will be discussed later in Section 4.2. The corresponding dynamics of $\tilde{\mathcal{B}}_E$ is $\mathcal{M}_n = (\mathcal{S}_n, \mathcal{A}_n, \mathcal{P}_n, r_n, \gamma, p_0^n)$, where $\mathcal{A}_n = \mathcal{A}$ as we ignore the noise on actions. For all $s, s' \in \mathcal{S}$ and $\tilde{s} = f_{\text{noise}}(s), \tilde{s}' = f_{\text{noise}}(s') \in \mathcal{S}_n$, we have $p_0(s) = p_0^n(\tilde{s})$, $\mathcal{P}(s, a, s') = \mathcal{P}(\tilde{s}, a, \tilde{s}')$ and $r(s, a) = r_n(\tilde{s}, a)$. The main challenge in LND is that the states $s \in \mathcal{S}_n$ and actions $a \in \mathcal{A}_n$ in the noisy expert's

¹For simplicity, we consider \mathcal{B}_E as a set of $T \times H$ (s, a) pairs.

MDP \mathcal{M}_n do not necessarily match the states $s \in \mathcal{S}$ and actions $a \in \mathcal{A}$ in the imitator's MDP \mathcal{M} .

4. Domain Adaptation for Noisy Expert Data

Although AIL has shown promising performance on various imitation learning tasks, it remains unclear whether it can solve the problem of LND where the expert and the imitator have different domains caused by noise. In the first part, we theoretically analyze the limitations of AIL methods (especially GAIL) in solving the LND problems. This explains why we need to introduce domain adaptation techniques. In the second part, we introduce the anchor buffer, a technique commonly used in domain adaptation methods, and analyze it in the context of LND.

4.1. Why do we need domain adaptation?

AIL can hardly solve LND problems, for it essentially attempts to justify expert data rather than exploring the logic behind expert behavior (Brown et al., 2019). To prove the limitations of the AIL methods in dealing with the LND problem, we start with GAIL and propose the following proposition:

Proposition 4.1. (*Limitation of GAIL*) *Given expert data with LTI noise and no perfect information, GAIL can only solve small-scale Gaussian noise and cannot handle other LTI noise, proof in Appendix B.*

To address the Imitation Learning problem with different domains between the expert and the imitator under the framework of AIL, we need to utilize consistent representations, which can be achieved by domain adaptation techniques. Domain adaptation methods aim to map the noisy expert domain and the noiseless imitator domain to the same latent space, thus reducing the LND problem to a simple IRL case.

4.2. Anchor buffer

Anchor buffer is a commonly used design in domain adaptation methods, which is also used in DIDA. We provide insights into understanding the necessity of the anchor buffer and analyze how the anchor buffer works under the LND setting.

Considering the simplest case in Figure 2, where the discriminator's classification boundary can be seen as a straight line, $\tilde{\mathcal{B}}_E$ and \mathcal{B}_I can be separated easily by any classification boundary with slope $k \in (-\infty, 0]$. So we need to construct a set of data within the noisy expert domain to aid in training, and we call such a dataset an **anchor buffer**. The anchor buffer acts as the bridge to connect the other two buffers: $\tilde{\mathcal{B}}_A$ and $\tilde{\mathcal{B}}_E$ belong to \mathcal{D}^{N} with the same noise level, and training a policy discriminator D_p with these two buffers allows D_p to categorize the data based on the expertise level

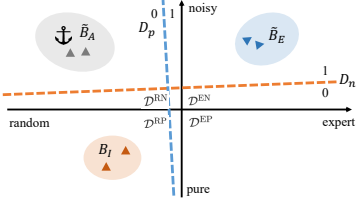


Figure 2. We consider the expertise level and the noise level of data as the x-axis and the y-axis, respectively. \tilde{B}_E and B_A are located at the diagonal position.

only; \tilde{B}_A and \tilde{B}_I belong to \mathcal{D}^R with the same expertise level, and thus guarantees a noise discriminator D_n to rely only on the noise level of the data for classification.

In addition, there are certain problems with the way that several previous domain adaptation methods construct their anchor buffers. For instance, DisentanGAIL (Cetin & Celiktutan, 2021) collects prior data by executing random behavior in both expert and imitator domains. TPIL (Stadie et al., 2017) also designs a similar dataset by executing random policies in the expert domain. The above two methods need interactions within the expert’s domain to collect prior data and we refer to this generation method of anchor buffer as *anchor-buffer-random*. In many IL scenarios, however, the imitator only has access to the expert demonstrations and cannot interact within the expert domain. Therefore, it is unrealistic to collect data through extra interactions. To address this problem, DIDA proposes a new method for constructing anchor buffers without pre-collected random data from the expert domain, which will be introduced in the next section.

5. A Practical Implementation of DIDA

In this section, we will detail our design of a denoised imitation learning method, DIDA. In Section 5.1, we introduce the components and the optimization objective of DIDA. In Section 5.2, we propose Domain Adversarial Sampling (DAS), which is an imbalanced sampling technique. In Section 5.3, we explain the design idea of a self-adaptive rate.

5.1. Components and Optimization objective

Inspired by the domain adaptation theory (Ben-David et al., 2006), we aim to learn a representation that is not discriminative between the noisy domain \mathcal{D}^N and the pure domain \mathcal{D}^P , but can still be used to perform IL tasks well. To achieve this goal, we design a feature encoder G_f to extract the state embedding $z_t = G_f(s_t)$, a noise discriminator D_n , and a policy discriminator D_p . In each iteration, we sample from B_I , \tilde{B}_A , and \tilde{B}_E to get corresponding state batches $S_I = \{s_i^I\}_{i=1}^N$, $\tilde{S}_A = \{s_i^A\}_{i=1}^N$, and $\tilde{S}_E = \{s_i^E\}_{i=1}^N$, re-

spectively. Then we use G_f to map these batches into the imitator embeddings $Z_I = \{z_i^I\}_{i=1}^N$, the noisy anchor embeddings $\tilde{Z}_A = \{z_i^A\}_{i=1}^N$ and the noisy expert embeddings $\tilde{Z}_E = \{z_i^E\}_{i=1}^N$, where $z_i^* = G_f(s_i^*)$. DIDA proposes two adversarial training branches: **Policy branch** takes policy π as the generator and combines G_f with D_p to distinguish whether z_t belongs to the anchor domain \mathcal{D}^R ; **Noise branch** takes G_f as the generator, and uses D_n to distinguish whether z_t belongs to the noisy domain \mathcal{D}^N . Well-trained discriminators should be orthogonal to the coordinate axes in Figure 2, and we expect D_p and D_n to make decisions independently.

Optimization objective of DIDA. For simplicity, we denote $\mathbb{E}_{s \sim \pi}[f(G_f(s))] = \mathbb{E}_{\pi}[f(z)] = \mathbb{E}_{B_I}[f(z)]$ where f can be any function, and abbreviate (z_t, z_{t+1}) as σ_t . Aiming to derive the optimization objective for the entire DIDA framework, we start with the policy branch and then introduce the noise branch. The optimization objective of the policy branch is:

$$\max_{\pi} \min_{D_p} \mathcal{L}_p = \mathbb{E}_{\pi \cup \tilde{\pi}_r}[\log(1 - D_p(\sigma_t))] \quad (3)$$

$$+ \mathbb{E}_{\tilde{\pi}_e}[\log D_p(\sigma_t)] \quad (4)$$

$$= \mathbb{E}_{\pi \cup \tilde{\pi}_r \cup \tilde{\pi}_e}[L_p(D_p(\sigma_t), p_{l_t})] \quad (5)$$

$$= \mathbb{E}[L_p(D_p(\sigma_t), p_{l_t})] \quad (6)$$

where L_p is the policy loss function, $l_t^p = \mathbb{I}(s_t \in \tilde{B}_A \cup B_I)$ is the policy domain label to separate \mathcal{D}^R and \mathcal{D}^E . \mathbb{I} is the indicator function. Equation (5) is computed over all datasets, so we drop its subscript for simplicity. To obtain domain-agnostic embeddings, we introduce the following mutual information term:

$$\max_{\pi} \min_{D_p} \mathcal{L}_p = \mathbb{E}[L_p(D_p(\sigma_t), l_t^p)] \quad (7)$$

$$\text{s.t. } MI(z, n_l) = 0 \quad (8)$$

where the noise domain label $l_t^n = \mathbb{I}(s \in \tilde{B}_E \cup \tilde{B}_A)$ is the indicator to separate \mathcal{D}^N and \mathcal{D}^P . The mutual information (MI) term forces G_f to learn embedding that is not discriminative between the noisy domain \mathcal{D}^N and the pure domain \mathcal{D}^P . DIDA instantiates the MI term with the noise discriminator D_n to maximize domain confusion:

$$\max_{\pi} \min_{D_p} \max_{D_n} \mathcal{L}_p + \mathcal{L}_n = \mathbb{E}[L_p(D_p(\sigma_t), l_t^p)] \quad (9)$$

$$+ L_n(D_n(z_t), l_t^n) \quad (10)$$

where L_n is the noise loss function and can have a different form than L_p . We apply the gradient flipped technique from (Ganin et al., 2016) to tackle the conflict of update goals between the noise discriminator and the feature encoder. Then the optimization objective becomes:

$$\max_{\pi} \min_{D_p, D_n, G_f} \mathcal{L}_p + \mathcal{L}_n = \mathbb{E}[L_p(D_p(\sigma_t), l_t^p)] \quad (11)$$

$$+ \lambda L_n(D_n(R(G_f(s_t))), l_t^n) \quad (12)$$

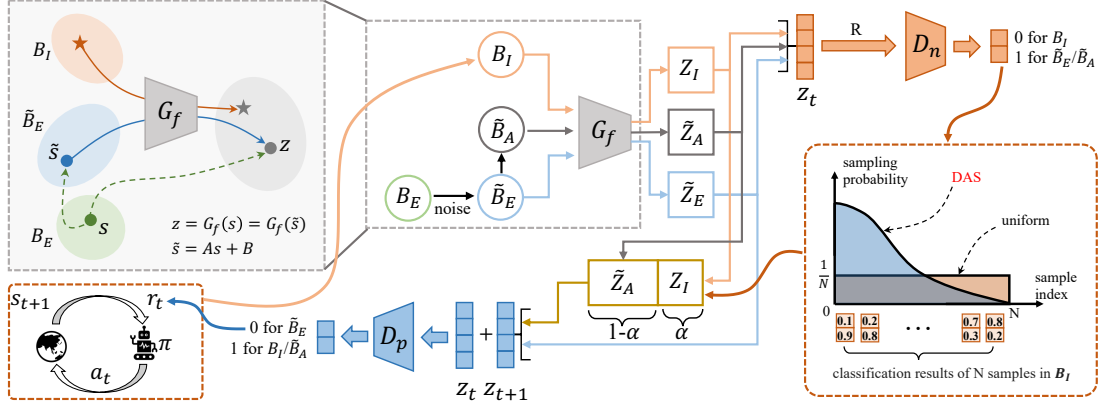


Figure 3. The main framework of the DIDA method. We design the feature encoder G_f to map state s into embedding z . We sample batches of size N in the imitator buffer B_I , the noisy anchor buffer \tilde{B}_A , and the noisy expert buffer \tilde{B}_E (defined in Section 3) and feeding them into G_f to get embeddings Z_I , \tilde{Z}_A , and \tilde{Z}_E . Noise discriminator D_n judges the noise level of all embeddings and generates binary classification results. R denotes the gradient reversal layer. We apply the technique of domain adversarial sampling (DAS, defined in Section 5.2) to compute the confusion probability distribution $P_{das}(z^I)$ over Z_I based on the classification error probability of the embeddings. We take αN embeddings from Z_I based on P_{das} and replace the αN embeddings in \tilde{Z}_A with them randomly, where α is the adaptive rate from Section 5.3. Policy discriminator D_p judges the expertise level of Z_{mix} and \tilde{Z}_E .

The gradient reversal layer R acts as an identity function in the forward propagation, while flips the sign of gradients in the backward propagation. Domain weight λ controls the trade-off between the two loss terms, which can be computed as Algorithm 1. According to (Cetin & Celiktutan, 2021), the information contained in z can be divided into the *domain information* and the *goal-completion information*. With the model converging, the correlation between the embedding z and the noise label l_t^n is minimized. In other words, domain information is eliminated as much as possible, leaving only the goal-completion information which is useful to the policy branch training.

New construction method of anchor buffer. We randomly shuffle the state-action pairs of the noisy expert buffer \tilde{B}_E to obtain the noisy random buffer (mentioned as the anchor buffer) $\tilde{B}_A = f_{\text{shuffle}}(\tilde{B}_E)$. We refer to this generation method as *anchor-buffer-shuffle*. We conduct ablation experiments in Section 6.2 to explore and compare the effects of different anchor buffer construction methods on experimental performance.

5.2. Domain Adversarial Sampling (DAS)

The imitator embeddings Z_I is an *imbalanced* dataset for the distribution of domain information is different across samples, which can be justified by the lower center figure of Figure 4. D_n distinguishes whether an embedding is from \mathcal{D}^N or \mathcal{D}^P based on the domain information, so the classification accuracy can be used to measure the amount of domain information in the embedding. High-accuracy samples are detrimental to policy branch training because they contain plenty of domain information. Therefore, we need to design

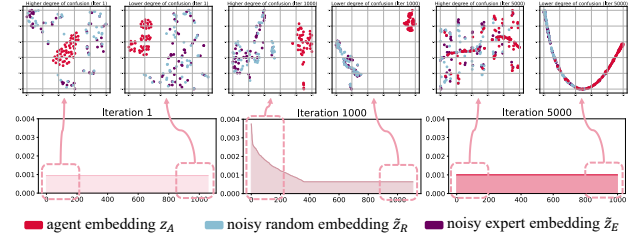


Figure 4. **Top:** The confusion probability P_{das} of Z_A at iter-1, iter-1000, and iter-5000 are shown from left to right, sorting the samples with their degrees of confusion decreasing from left to right. **Bottom:** The t-SNE plots of embeddings from Z_A , \tilde{Z}_R , and \tilde{Z}_E at iter-1000. From left to right corresponds to embeddings with the highest, middle, and lowest degrees of confusion at iter-1000, respectively. More detailed t-SNE plots in Appendix C.4.

an imbalanced sampling method rather than uniform sampling to extract samples with less domain information in Z_I and use these samples to train the policy discriminator. We define the following confusion probability:

$$P_{das}(z_i^I) = \frac{p_i}{\sum_{j=1}^N p_j} \quad (13)$$

$$\text{where } p_i = P(D_n(z_i^I) = 1), \forall z_i^I \in Z_I \quad (14)$$

We refer to $P_{das}(z_i^I)$ as the *degree of confusion* of z_i^I . We take αN embeddings from Z_I based on P_{das} and replace the αN embeddings in \tilde{Z}_A with them randomly. Then we use the obtained mixed embeddings Z_{mix} to train the policy discriminator.

As shown in the bottom rows of Figure 4, the confusion

probabilities of iter-1 and iter-5000 are both nearly uniform distributions. Because no prior knowledge is introduced at iter-1, D_n classifies all embeddings into the same class with approximately equal probabilities and the domain confusion is maximized. At iter-5000, all domain information is eliminated from embeddings, at which point D_n is confused about the domains and performs similar to in iter-1. In the top rows of Figure 4, samples with greater degrees of confusion are closer to each other in different clusters.

5.3. Self-Adaptive Rate (SAR)

The Z_{mix} used for training the policy discriminator is composed of Z_I and \tilde{Z}_A . The proportion of embeddings from Z_I needed at different stages of training is not the same, so we design the adaptive rate α to control this proportion. We define p_{acc} as the classification accuracy of D_n on all data, and define α as a function of p_{acc} :

$$\alpha = f_{\alpha}(p_{\text{acc}}) \quad (15)$$

$$= \mathbb{I}(p_{\text{acc}} > p) \frac{1 - p_{\text{acc}}}{1 - p} + \mathbb{I}(p_{\text{acc}} \leq p) \frac{p_{\text{acc}}}{p} \quad (16)$$

where f_{α} is the adaptive function. p is a hyperparameter and DIDA sets it as $\frac{2}{3}$ (can also be denoted as SAR- $\frac{2}{3}$). The value comes from the proportion of noisy data in all data ($|\tilde{Z}_E| + |\tilde{Z}_A| / (|\tilde{Z}_E| + |\tilde{Z}_A| + |Z_I|) = \frac{2}{3}$). We perform ablation in Section 6.2 for different settings of p . The adaptive rate behaves as a linear function in both $[0, p]$ and $[p, 1]$. $\alpha \in [0, 1]$ reaches its maximum value of 1 at $p_{\text{acc}} = p$, and reaches the minimum value of 0 at $p_{\text{acc}} = 0$ or 1.

Our design concerning f_{α} is explained below. Flipping the output of a classifier with $p_{\text{acc}} = 1$ turns it into a classifier with $p_{\text{acc}} = 0$, demonstrating that achieving low accuracy still requires much domain information. Thus too high or too low classification accuracy of D_n indicates that G_f fails to remove the domain information from embeddings. In this case, we reduce the proportion of Z_I , and use more of \tilde{Z}_A and \tilde{Z}_E as input which can prevent D_p from gaining the ability to classify through domain information.

Figure 5 shows two intriguing phenomena: **(1)** The value of p_{acc} is mostly $p_1 = \frac{1}{3}$ and $p_2 = \frac{2}{3}$ at iter-1. **(2)** p_{acc} fluctuates rapidly and regularly between p_1 and p_2 in the late stage of training. The top plotting in Figure 5 explains the first phenomenon: after randomly initializing the parameters, D_n will most likely classify the three datasets into the same category 0 or 1 (0 corresponds to $p_{\text{acc}} = p_1$, and 1 corresponds to $p_{\text{acc}} = p_2$). Thus we believe that p_1 and p_2 are special accuracy values that correspond to the random classification results without any prior knowledge. Then we attempt to explain the second phenomenon. With the model converging, we expect G_f to eliminate all domain information of the state embeddings, and thus satisfy $MI(z, l_t^n) = 0$. At this time, D_n classifies randomly simi-

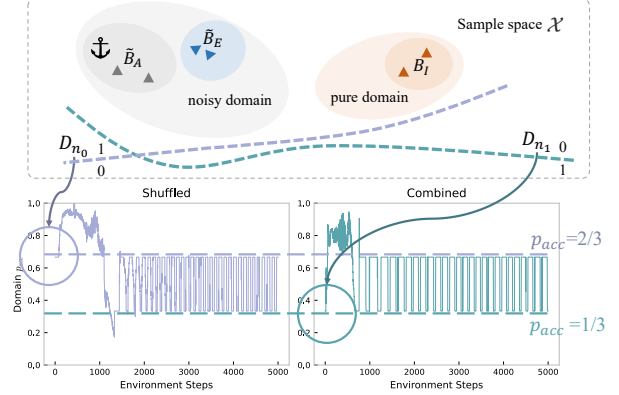


Figure 5. Curve of change in p_{acc} . **Top:** B_I , \tilde{B}_A and \tilde{B}_E only occupy a tiny portion of the n -dimensional state space \mathcal{X} . When D_n is randomly initialized, the classification hyperplane has a high probability of classifying all datasets into the same category, resulting in an accuracy of $\frac{2}{3}$ (e.g. D_{n_0}) or $\frac{1}{3}$ (e.g. D_{n_1}). **Bottom Left:** The initial value is p_2 , and it fluctuates between p_1 and p_2 in the late stage of training. **Bottom Right:** The initial value is p_1 and it also fluctuates between p_1 and p_2 .

larly to the iter-1 moment, thus p_{acc} fluctuates between p_1 and p_2 . Results in Figure 4 also verify these phenomena.

6. Experiments

We conduct several experiments to answer the following scientific questions:

- (1) Can DIDA** achieve excellent performance in different environments and under various noise?
- (2) How** do the different components of DIDA contribute to the final performance?
- (3) What** are the effects of different types of noise on imitation learning? Can we extract useful information about imitating noisy demonstrations?

Datasets Preparation. We test the ability of DIDA and other baseline methods with two control tasks from MuJoCo (Todorov et al., 2012): *Hopper* and *Swimmer*. Firstly, we run PPO (Schulman et al., 2017) on each environment for 1000 episodes to obtain the expert policy π^E , compute its test return for 100 episodes, and record its performance. Then we collect 50 episodes of expert buffer \mathcal{B}_E with the expert policy. Finally, to simulate the noise introduced during data transmission, we add various noise on \mathcal{B}_E to create corresponding noisy expert buffers. It is worth mentioning that we set $\mu = 0$ and $\sigma = 0.1$ for *Gaussian* noise; we split \mathcal{B}_E into four parts randomly and evenly, add four different noise to each part, and combine them to create the buffer of *Combined* noise.

Table 1. Test returns of DIDA and the other baseline methods on two MuJoCo environments with five noise. Each combination of environment and noise type is considered as a task (12 tasks in total). The table reports the mean (higher is better) and standard deviation of the return evaluated on all tasks for each method over three trials.

Env	Noise	DIDA(ours)	GWIL	SAIL	TPIL	GAIL	BC
Hopper (Expert:1813.6±590.5)	None	1311.0±518.6	694.4±300.6	-18.4±1.1	1506.3±795.2	1708.4±436.8	1605.8±489.0
	Shuffle	2248.1±475.8	822.6±224.7	21.9±1.0	573.9±354.2	316.1±463.0	76.1±98.6
	Doubly-stochastic	1598.6±939.3	955.4±256.1	0.7±0.1	974.1±913.7	447.4±165.7	1.7±3.0
	Normal	1271.8±618.2	675.7±367.4	-95.3±15.4	560.9±344.6	458.6±348.6	4.4±1.1
	Gaussian	2284.4±807.2	873.2±248.5	1021.5±0.3	573.1±337.4	454.9±303.6	89.6±31.3
	Combined	2340.6±808.3	939.6±187.0	-91.8±44.2	483.7±237.9	402.2±156.7	141.9±69.4
Swimmer (Expert:122.8±1.7)	None	120.8±1.8	5.0±11.9	-71.4±55.9	117.5±6.1	119.6±3.7	122.8±2.4
	Shuffle	93.0±36.6	1.5±18.1	-6.6±7.9	31.9±41.4	38.0±14.5	17.0±6.2
	Doubly-stochastic	74.4±18.0	-1.6±13.6	1.7±18.1	-1.1±14.7	69.8±8.3	-46.6±45.0
	Normal	39.8±13.5	0.8±12.2	-16.9±6.4	27.9±15.4	21.4±23.5	17.9±17.3
	Gaussian	72.0±35.5	-3.1±11.0	-6.7±8.8	57.5±23.7	43.6±38.3	36.1±5.9
	Combined	62.2±12.7	-3.6±15.1	17.5±12.7	37.6±31.7	49.3±12.1	32.0±4.6

Baselines. We compare our method to 5 baselines detailed in Appendix D.1. BC takes a supervised learning way to learn a policy that maps states to actions using expert demonstrations. IRL methods like GAIL (Ho & Ermon, 2016) adopt the idea of GAN (Goodfellow et al., 2014) and learn a policy distribution by generating state-action pairs that are indistinguishable from those of an expert policy, TPIL (Stadie et al., 2017) addresses the domain gap by aligning the domains of the expert and the learner in the third-person imitation learning setting, while GWIL (Fickinger et al., 2021) uses the Gromov-Wasserstein distance to align and compare states between the different spaces of the agents. Moreover, SAIL (Liu et al., 2019) is a state adaptation-based algorithm that addresses the problem of different dynamics models between the imitator and the expert. TPIL, GWIL and SAIL all utilize domain adaptation just as DIDA. Since in our setting noise is only added to states, it’s worth exploring if SAIL can work well on LND problems.

6.1. Can DIDA achieve excellent performance in different environments and under various noise?

We evaluate DIDA and other baseline methods on tasks across different environments and noise. Results in Table 1 shows that DIDA significantly outperforms other baselines under all noise conditions, and achieves comparable results to the best baseline on the pure expert cases, demonstrating the effectiveness of domain adaptation between agent domain and noise domain. DIDA generally performs better on Hopper than on Swimmer, especially achieving better than expert performance under *Shuffle*, *Guassian* and *Combine* noise. BC simply learns a mapping from the noisy state space \mathcal{S}_n to the action space \mathcal{A}_n using supervised learning paradigm. The learned policy has almost no noise resistance, so although it performs well in the pure expert case,

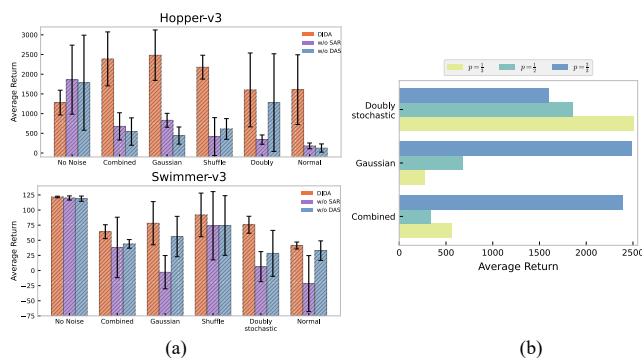


Figure 6. (a): Results of ablation studies of SAR and DAS with all noises on Hopper and Swimmer. (b): Performances of ablation studies on different settings of p in SAR.

it performs much worse in all noisy cases. As a domain adaptation method, TPIL has a certain degree of noise resistance. However, due to the lack of self-adaptive designing, its performance is inferior to DIDA. GAIL’s performance is roughly comparable to TPIL’s, as it simply attempts to align expert data rather than extracting expertise knowledge behind expert behavior. GWIL’s performance is quite good on Hopper, but it gets relatively low returns on Swimmer. SAIL also cannot handle noisy demonstrations very well. These results show that our proposed method, DIDA, can achieve robust good performance on almost all designed tasks compared to other domain adaptation methods.

6.2. How do the different components of DIDA contribute to final performance?

To evaluate the contribution of different components of DIDA, we conduct ablation studies on the domain adversar-

ial sampling (DAS), the self-adaptive rate (SAR), and the anchor buffer \tilde{B}_A . We also explore different initialization of p defined in Section 5.3 to show its effect.

Ablation on DAS and SAR. To investigate the individual effects of DAS and SAR, we conduct ablations on each separately with all noise on both Hopper and Swimmer environments. As shown in Figure 6-(a), removing SAR leads to a significant performance drop on Hopper and a high variance of performance on Swimmer, indicating that dynamically adjusting the proportion of Z_I in Z_{mix} can help assign better training samples to the policy discriminator thus improving the performance and the stability of the algorithm. Eliminating DAS results in a drastic decrease in performance, revealing that compared with uniform sampling, DAS can select embeddings with less domain information thus facilitating the training process. In the case of pure expert, w/o SAR and w/o DAS achieve comparable performance to DIDA, suggesting that our method is somehow modular-robust and the performance is desirable in the pure expert case even if SAR or DAS is absent. w/o DAS has the SAR module, while w/o SAR does not because DAS is SAR-dependent. We observe that w/o DAS performs better than w/o SAR in most cases, which also validates the effectiveness of the SAR design.

Different generation methods of \tilde{B}_A . Considering the following two different generation methods of anchor buffer: *anchor-buffer-random* collects data in the noise domain using a random policy, which is adopted in previous works; while DIDA proposes *anchor-buffer-shuffle*, which shuffles the noisy expert buffer randomly to simulate noisy random data. As illustrated in Figure 7, *anchor-buffer-random*(AB-random) and *anchor-buffer-shuffle*(AB-shuffle) exhibit a negligible impact on TPIL’s performance. This demonstrates that this simple data generation method is efficient. It also indirectly validates the effectiveness of other designs of DIDA including DAS and SAR. Agent-environment interaction is expensive in most real-world scenarios, making it impractical for AB-random to collect data in the expert domain. In contrast, AB-shuffle only requires a shuffling operation on the noisy expert buffer. While achieving comparable performance, our AB-shuffle method is more practical than AB-random in real-world applications.

Different settings of SAR. We investigate the effects of different settings of p in SAR on experimental performance. We test SAR- $\frac{1}{3}$, SAR- $\frac{1}{2}$ and SAR- $\frac{2}{3}$ on three kinds of noise. As shown in Figure 6-(b) DIDA’s default setting SAR- $\frac{2}{3}$ outstrips other settings on two noise, indicating the rationality of using the proportion of noisy data as the value of p . SAR- $\frac{1}{3}$ performs best with the last noise, suggesting that both $p_{acc} = \frac{1}{3}$ and $p_{acc} = \frac{2}{3}$ correspond to cases where the discriminator is unable to separate the data, which is consistent with the analysis in Section 5.3.

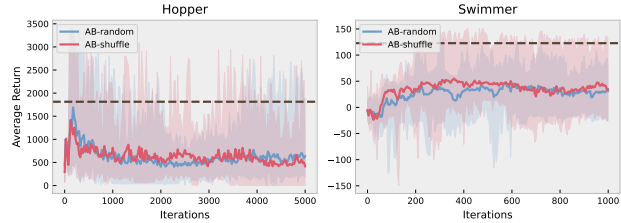


Figure 7. Performance curves of TPIL with two different anchor buffer generation methods. We conduct experiments on all noise types in two environments and present the overall average performance, where the dotted line represents the expert performance. Performance plots for each noise separately are in Appendix C.2.

6.3. Effects of different noise

Although DIDA performs well almost on all designed tasks, it still shows variance across different noise. The additive *Gaussian* noise is relatively simple, and we conduct a simple experiment using GAIL to imitate expert demonstrations under different scales of Gaussian noise. The results in Figure 8 demonstrate that the performance of GAIL remains satisfying when the noise scale is relatively small, but decreases with the noise scale increasing.

The multiplicative noise has a greater impact on algorithm performance. We find that if the algorithm can achieve better performance on *Doubly-stochastic* noise, then the performance on *Shuffle* can also be guaranteed, which is consistent with the definition of the two noise in Section 3. *Normal* noise is the hardest not only for DIDA, but for other baseline methods on the two environments.

7. Conclusion

Our work focuses on scenarios where pure expert data or human ranking is inaccessible, thus imitator must learn from many types of noisy data. We propose Denoised Imitation learning based on Domain Adaptation (DIDA), which designs a feature encoder trying to extract task-related but domain-agnostic information from the noisy states and eliminate domain information with the help of a noise discriminator and a policy discriminator. To facilitate training, we design several efficient modules including a shuffle anchor buffer, a self-adaptive rate and a domain-adversarial sampling technique. Our experiments validate the effectiveness of our designed modules and further demonstrate the impact of various noise.

Limitations and Future Work. DIDA has addressed several LTI noise, and future work could consider time-varying noise and even nonlinear noise. We assume that noise can be divided into the task-irrelevant part and the task-relevant part, and focus on the task-irrelevant noise added during

signal transmission. Yet task-relevant noise is inherent in the environment, which can affect the accuracy of an imitator’s perception of the real world. To solve the task-relevant noise may be a promising research field in future works.

8. Societal Impact

This paper presents work that aims to advance the field of Machine Learning. There are many potential societal consequences of our work, none of which we feel must be specifically highlighted here.

References

- Belkhale, S., Cui, Y., and Sadigh, D. Hydra: Hybrid robot actions for imitation learning. In *Conference on Robot Learning*, pp. 2113–2133. PMLR, 2023.
- Ben-David, S., Blitzer, J., Crammer, K., and Pereira, F. Analysis of representations for domain adaptation. *Advances in neural information processing systems*, 19, 2006.
- Brown, D., Goo, W., Nagarajan, P., and Niekum, S. Extrapolating beyond suboptimal demonstrations via inverse reinforcement learning from observations. In *International conference on machine learning*, pp. 783–792. PMLR, 2019.
- Brown, D. S., Goo, W., and Niekum, S. Better-than-demonstrator imitation learning via automatically-ranked demonstrations. In *Conference on robot learning*, pp. 330–359. PMLR, 2020.
- Burchfiel, B., Tomasi, C., and Parr, R. Distance minimization for reward learning from scored trajectories. In *Proceedings of the AAAI Conference on Artificial Intelligence*, volume 30, 2016.
- Cetin, E. and Celiktutan, O. Domain-robust visual imitation learning with mutual information constraints. *arXiv preprint arXiv:2103.05079*, 2021.
- Chae, J., Han, S., Jung, W., Cho, M., Choi, S., and Sung, Y. Robust imitation learning against variations in environment dynamics. In *International Conference on Machine Learning*, pp. 2828–2852. PMLR, 2022.
- Chen, L., Paleja, R., and Gombolay, M. Learning from sub-optimal demonstration via self-supervised reward regression. In *Conference on robot learning*, pp. 1262–1277. PMLR, 2021.
- Chen, M., Bai, Y., Poor, H. V., and Wang, M. Efficient rl with impaired observability: Learning to act with delayed and missing state observations. *arXiv preprint arXiv:2306.01243*, 2023.
- Davis, G. P., Katz, G. E., Gentili, R. J., and Reggia, J. A. Neuroceril: Robotic imitation learning via hierarchical cause-effect reasoning in programmable attractor neural networks. *International Journal of Social Robotics*, pp. 1–19, 2023.
- Duan, A., Batzianoulis, I., Camoriano, R., Rosasco, L., Pucci, D., and Billard, A. A structured prediction approach for robot imitation learning. *The International Journal of Robotics Research*, pp. 02783649231204656, 2023.
- Fickinger, A., Cohen, S., Russell, S., and Amos, B. Cross-domain imitation learning via optimal transport. *arXiv preprint arXiv:2110.03684*, 2021.
- Gandhi, K., Karamcheti, S., Liao, M., and Sadigh, D. Eliciting compatible demonstrations for multi-human imitation learning. In *Conference on Robot Learning*, pp. 1981–1991. PMLR, 2023.
- Ganin, Y., Ustinova, E., Ajakan, H., Germain, P., Larochelle, H., Laviolette, F., March, M., and Lempitsky, V. Domain-adversarial training of neural networks. *Journal of machine learning research*, 17(59):1–35, 2016.
- Ghasemipour, S. K. S., Zemel, R., and Gu, S. A divergence minimization perspective on imitation learning methods. In *Conference on Robot Learning*, pp. 1259–1277. PMLR, 2020.
- Goodfellow, I., Pouget-Abadie, J., Mirza, M., Xu, B., Warde-Farley, D., Ozair, S., Courville, A., and Bengio, Y. Generative adversarial nets. *Advances in neural information processing systems*, 27, 2014.
- Gu, A. and Dao, T. Mamba: Linear-time sequence modeling with selective state spaces. *arXiv preprint arXiv:2312.00752*, 2023.
- Haliem, M., Bonjour, T., Alsalem, A., Thomas, S., Li, H., Aggarwal, V., Bhargava, B., and Kejriwal, M. Learning monopoly gameplay: A hybrid model-free deep reinforcement learning and imitation learning approach. *arXiv preprint ArXiv:2103.00683*, 2021.
- Ho, J. and Ermon, S. Generative adversarial imitation learning. *Advances in neural information processing systems*, 29, 2016.
- Hussein, A., Gaber, M. M., Elyan, E., and Jayne, C. Imitation learning: A survey of learning methods. *ACM Computing Surveys (CSUR)*, 50(2):1–35, 2017.
- Ke, L., Choudhury, S., Barnes, M., Sun, W., Lee, G., and Srinivasa, S. Imitation learning as f-divergence minimization. In *Algorithmic Foundations of Robotics XIV*:

- Proceedings of the Fourteenth Workshop on the Algorithmic Foundations of Robotics 14*, pp. 313–329. Springer, 2021.
- Langley, P. Crafting papers on machine learning. In Langley, P. (ed.), *Proceedings of the 17th International Conference on Machine Learning (ICML 2000)*, pp. 1207–1216, Stanford, CA, 2000. Morgan Kaufmann.
- Laskey, M., Lee, J., Fox, R., Dragan, A., and Goldberg, K. Dart: Noise injection for robust imitation learning. In *Conference on robot learning*, pp. 143–156. PMLR, 2017.
- Liu, F., Ling, Z., Mu, T., and Su, H. State alignment-based imitation learning. *arXiv preprint arXiv:1911.10947*, 2019.
- Osa, T., Pajarinen, J., Neumann, G., Bagnell, J. A., Abbeel, P., Peters, J., et al. An algorithmic perspective on imitation learning. *Foundations and Trends® in Robotics*, 7 (1-2):1–179, 2018.
- Peng, Y.-L. and Lee, W.-P. Valuation of stocks by integrating discounted cash flow with imitation learning and guided policy. *IEEE Transactions on Automation Science and Engineering*, 2023.
- Ross, S. and Bagnell, D. Efficient reductions for imitation learning. In *Proceedings of the thirteenth international conference on artificial intelligence and statistics*, pp. 661–668. JMLR Workshop and Conference Proceedings, 2010.
- Schaal, S. Is imitation learning the route to humanoid robots? *Trends in cognitive sciences*, 3(6):233–242, 1999.
- Schulman, J., Wolski, F., Dhariwal, P., Radford, A., and Klimov, O. Proximal policy optimization algorithms. *arXiv preprint arXiv:1707.06347*, 2017.
- Sharma, P., Pathak, D., and Gupta, A. Third-person visual imitation learning via decoupled hierarchical controller. *Advances in Neural Information Processing Systems*, 32, 2019.
- Shi, Z., Xu, Y., Fang, M., and Chen, L. Self-imitation learning for action generation in text-based games. In *Proceedings of the 17th Conference of the European Chapter of the Association for Computational Linguistics*, pp. 703–726, 2023.
- Stadie, B. C., Abbeel, P., and Sutskever, I. Third-person imitation learning. *arXiv preprint arXiv:1703.01703*, 2017.
- Tangkaratt, V., Charoenphakdee, N., and Sugiyama, M. Robust imitation learning from noisy demonstrations. *arXiv preprint arXiv:2010.10181*, 2020.
- Todorov, E., Erez, T., and Tassa, Y. Mujoco: A physics engine for model-based control. In *2012 IEEE/RSJ international conference on intelligent robots and systems*, pp. 5026–5033. IEEE, 2012.
- Van der Maaten, L. and Hinton, G. Visualizing data using t-sne. *Journal of machine learning research*, 9(11), 2008.
- Wang, J., Zhuang, Z., Wang, Y., and Zhao, H. Adversarially robust imitation learning. In *Conference on Robot Learning*, pp. 320–331. PMLR, 2022.
- Wu, Y.-H., Charoenphakdee, N., Bao, H., Tangkaratt, V., and Sugiyama, M. Imitation learning from imperfect demonstration. In *International Conference on Machine Learning*, pp. 6818–6827. PMLR, 2019.
- Yuan, Y., Li, X., Heng, Y., Zhang, L., and Wang, M. Good better best: Self-motivated imitation learning for noisy demonstrations. *arXiv preprint arXiv:2310.15815*, 2023.
- Zhang, S., Cao, Z., Sadigh, D., and Sui, Y. Confidence-aware imitation learning from demonstrations with varying optimality. *Advances in Neural Information Processing Systems*, 34:12340–12350, 2021.
- Zhang, T. T., Kang, K., Lee, B. D., Tomlin, C., Levine, S., Tu, S., and Matni, N. Multi-task imitation learning for linear dynamical systems. In *Learning for Dynamics and Control Conference*, pp. 586–599. PMLR, 2023.

A. Algorithm

Algorithm 1 DIDA: Denoised Imitation Learning based on Domain Adaptation

Input: Expert buffer \mathcal{B}_E , empty buffers $\{\tilde{\mathcal{B}}_E, \tilde{\mathcal{B}}_A, \mathcal{B}_I\}$, noise operator f_{noise} and initial domain weight λ_0

- 1: Randomly initialize feature encoder G_f , policy net π , value net V_θ and discriminators $\{D_n, D_p\}$
- 2: $\tilde{\mathcal{B}}_E = f_{\text{noise}}(\mathcal{B}_E)$, and randomly shuffle $\tilde{\mathcal{B}}_E$ to get $\tilde{\mathcal{B}}_A$
- 3: **for** epoch $i = 1 : M$ **do**
- 4: Sample a batch of indexes from $|\tilde{\mathcal{B}}_E|$ and extract corresponding data in $\tilde{\mathcal{B}}_E$ and $|\tilde{\mathcal{B}}_A|$ to get \tilde{S}_E and \tilde{S}_A
- 5: **// Collect training data through interacting with environment**
- 6: $\mathcal{B}_I = \{s_t, a_t, r_t, s_{t+1}\}_{t=1}^N$, where $a_t \sim \pi^i(s_t)$, $h_t = \text{concat}(G_f(s_t), G_f(s_{t+1}))$ and $r_t = D_p(h_t)$
- 7: Extract states from \mathcal{B}_I to get $S_I = \{s_t, s_{t+1}\}_{t=1}^N$
- 8: Compute values $V_i = \{V_\theta^i(s_t)\}_{t=1}^N$, returns $G_i = \{\sum_{j=1}^t \gamma^j r_j\}_{t=1}^N$ and advantages $A_i = \{a_t\}_{t=1}^N$
- 9: Get embeddings $(Z_I, \tilde{Z}_E, \tilde{Z}_A)$ by feeding $(S_I, \tilde{S}_E, \tilde{S}_A)$ into G_f
- 10: **// Update noise and policy discriminators**
- 11: Compute loss between predictions $D_n(Z_I, \tilde{Z}_E, \tilde{Z}_A)$ and labels (0 for Z_I , 1 for \tilde{Z}_E and \tilde{Z}_A)
- 12: Compute the gradients g_n and perform backpropagation to update D_n
- 13: Calculate the adaptive rate α using the method described in Section 5.3
- 14: Compute the domain weight $\lambda = \lambda_0(2/(1 + e^{-10q}) - 1)$, where $q = \frac{i}{M}$
- 15: $Z_{\text{mix}} = \text{DAS}(\tilde{Z}_A, Z_I, \alpha)$
- 16: Compute loss between predictions $D_p(\tilde{Z}_E, Z_{\text{mix}})$ and labels (0 for Z_{mix} and 1 for \tilde{Z}_E)
- 17: Compute the gradients g_p and perform backpropagation to update D_p
- 18: **// Update feature encoder**
- 19: Use $g_p - \lambda g_n$ to update G_f , where negative sign comes from reverse gradient layer R
- 20: **// Perform PPO update**
- 21: $\pi^{i+1}, V_\theta^{i+1} = \text{ppo.update}(\pi^i, V_\theta^i, \mathcal{B}_I, G_i, A_i)$
- 22: **end for**

B. Proof

Proof of Proposition 4.1. GAIL (Ho & Ermon, 2016) has proved that a policy and its occupancy measure are one-to-one, and they can be converted into each other under the same MDP assumption. GAIL indirectly imitates an expert policy by matching the occupancy measures (Ho & Ermon, 2016). When the discriminator is unable to distinguish between the two distributions and the agent achieves a high return in evaluation, we believe that the agent has learned a policy that is close to the expert policy. However, the LND problem involves two different MDPs \mathcal{M} and \mathcal{M}_n . We believe that, under the influence of LTI noise, there exists a certain correspondence between the expert policy π_e (derived from dataset \mathcal{B}_E) in the original MDP \mathcal{M} and the noisy expert policy $\tilde{\pi}_e$ (derived from dataset $\tilde{\mathcal{B}}_E$) in the noisy MDP \mathcal{M}_n . The properties of LTI noise imply $\pi_e(s|a) = \tilde{\pi}_e(a|\tilde{s})$. We try to prove the following equation:

$$P(s_t = s|\pi_e) = P(s_t = \tilde{s}|\tilde{\pi}_e) \quad (17)$$

Let's prove it by mathematical induction, first considering the case $t = 0$, easily we can get:

$$P(s_0 = s|\pi_e) = p_0(s) = p_0^n(\tilde{s}) = P(s_0 = \tilde{s}|\tilde{\pi}_e) \quad (18)$$

where $\tilde{s} = f_{\text{noise}}(s)$, and Equation (18) holds for all $s \in \mathcal{S}$. We assume that the equation holds for $t = n - 1$, let us consider the case of $t = n$:

$$P(s_n = s|\pi_e) = \sum_{s'} P(s_{n-1} = s'|\pi_e) \sum_a \pi_e(a|s') \mathcal{P}(s|s', a) \quad (19)$$

$$= \sum_{s'} P(s_{n-1} = s'|\pi_e) \sum_a \tilde{\pi}_e(a|\tilde{s}') \mathcal{P}_n(\tilde{s}|s', a) \quad (20)$$

$$= \sum_{\tilde{s}'} P(s_{n-1} = \tilde{s}'|\tilde{\pi}_e) \sum_a \tilde{\pi}_e(a|\tilde{s}') \mathcal{P}_n(\tilde{s}|\tilde{s}', a) \quad (21)$$

$$= P(s_n = \tilde{s}|\tilde{\pi}_e) \quad (22)$$

Thus we finish the proof of Equation (17). Considering the definitions of ρ_e and $\tilde{\rho}_e$, we have:

$$\rho_{\pi_e}(s, a) = (1 - \gamma)\pi_e(a|s) \sum_{t=0}^{\infty} \gamma^t P(s_t = s | \pi_e) \quad (23)$$

$$= (1 - \gamma)\tilde{\pi}_e(a|\tilde{s}) \sum_{t=0}^{\infty} \gamma^t P(s_t = \tilde{s} | \tilde{\pi}_e) \quad (24)$$

$$= \rho_{\tilde{\pi}_e}(\tilde{s}, a) \quad (25)$$

LTI noise serves as a one-to-one mapping between s and \tilde{s} , so $\pi_e(a|s) = \tilde{\pi}_e(s|\tilde{s})$. Combining this with Equation (17), we can get Equation (25). That is, although the occupation measures of the two policies may be equal $\rho_e(s, a) = \tilde{\rho}_e(f_{\text{noise}}(s), a)$, they are actually two completely different policies. Directly using dataset $\tilde{\mathcal{B}}_E$ and dataset \mathcal{B}_A for GAIL learning would lead to training failure due to the gap between MDPs. Under the same MDP, $\rho(s, a) = \rho_e(s, a)$ and $\pi = \pi_e$ both are necessary and sufficient conditions for each other for the training of GAIL. Therefore, only if $\rho_e(\tilde{s}, a)$ is as close to $\rho_e(s, a)$ as possible can GAIL solve the LND problem, and the difference between the two measures the gap between MDPs. We now analyze the feasibility of this condition:

$$\rho_{\pi_e}(\tilde{s}, a) = (1 - \gamma)\pi_e(a|\tilde{s}) \sum_{t=0}^{\infty} \gamma^t P(s_t = \tilde{s} | \pi_e) \quad (26)$$

$$= (1 - \gamma)\pi_e(a|s) \sum_{t=0}^{\infty} \gamma^t P(s_t = s | \pi_e) \frac{\pi_e(a|\tilde{s})}{\pi_e(a|s)} |A^{-1}| \quad (27)$$

$$= \rho_{\pi_e}(s, a) \frac{\pi_e(a|\tilde{s})}{\pi_e(a|s)} |A^{-1}| \quad (28)$$

$$=^* \rho_{\pi_e}(s, a) \frac{\pi_e(a|\tilde{s})}{\pi_e(a|s)} \quad (29)$$

$$=^* \rho_{\pi_e}(s, a) \quad (30)$$

Equation (26) follows from the definition of occupancy measure, and Equation (27) is based on the probability density transformation formula $P(\tilde{s}) = P(f_{\text{noise}}^{-1}(\tilde{s})) |(f_{\text{noise}}^{-1})'(\tilde{s})|$. Only under the *Gaussian* noise or the special case of the *Doubly-stochastic* noise (the identity matrix is a type of doubly-stochastic matrix), A satisfies the requirements of an identity matrix, and Equation (29) holds. The validity of Equation (30) requires either of the following two conditions:

- 1) Expert π_e is robust to noise. For example, human experts can see the essence of the phenomenon when facing problems, and then make correct decisions.
- 2) The noise added is relatively small compared to the original state, such as Gaussian noise with small μ and σ . Then the agent can take similar action for the noisy state \tilde{s} and original state s .

Only if the noise is small enough to satisfy the second condition and the Equation (30) holds, GAIL can solve this case. Otherwise, the fraction term $\frac{\pi_e(a|\tilde{s})}{\pi_e(a|s)}$ cannot be ignored, then $\rho_{\pi_e}(\tilde{s}, a) \neq \rho_{\pi_e}(s, a)$ and GAIL cannot learn well. \square

In the above derivation, we found that two factors affect the difficulty of solving LND problem: the first is $|A^{-1}|$, which is determined by the nature of the problem itself; the second is $\frac{\pi_e(a|\tilde{s})}{\pi_e(a|s)}$, which can characterize the ability of the expert policy to resist noise. If we can estimate the value of $\frac{\pi_e(a|\tilde{s})}{\pi_e(a|s)}$ through importance sampling or off-policy techniques, it may help solve the LND problem. To verify the correctness of Proposition 4.1, we evaluated the performance of GAIL on different scales of *Gaussian* noise. We fixed the mean of the noise to 0 and set the standard deviation to 0.1, 0.5, and 1.0 respectively. As can be seen from Figure 8, the policy can resist noise with the scale of 0.1, so it satisfies $\pi_e(a|s) \approx \pi_e(s|\tilde{s})$ and the final performance can be guaranteed. As the noise scale increases, the performance of GAIL gradually deteriorates, which is consistent with the result of Proposition 4.1.

GAIL Performance Under Different Scales of Gaussian Noises

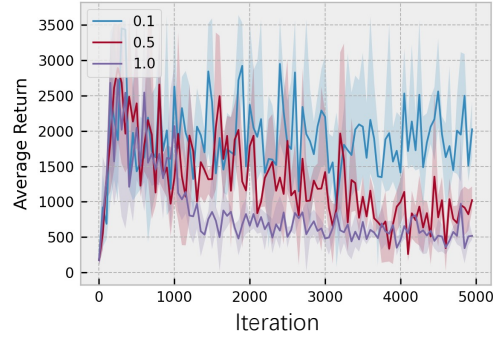


Figure 8. Performance of GAIL on different scales of **Gaussian** noise.

C. Additional results

C.1. Performance curves of Section 6.1

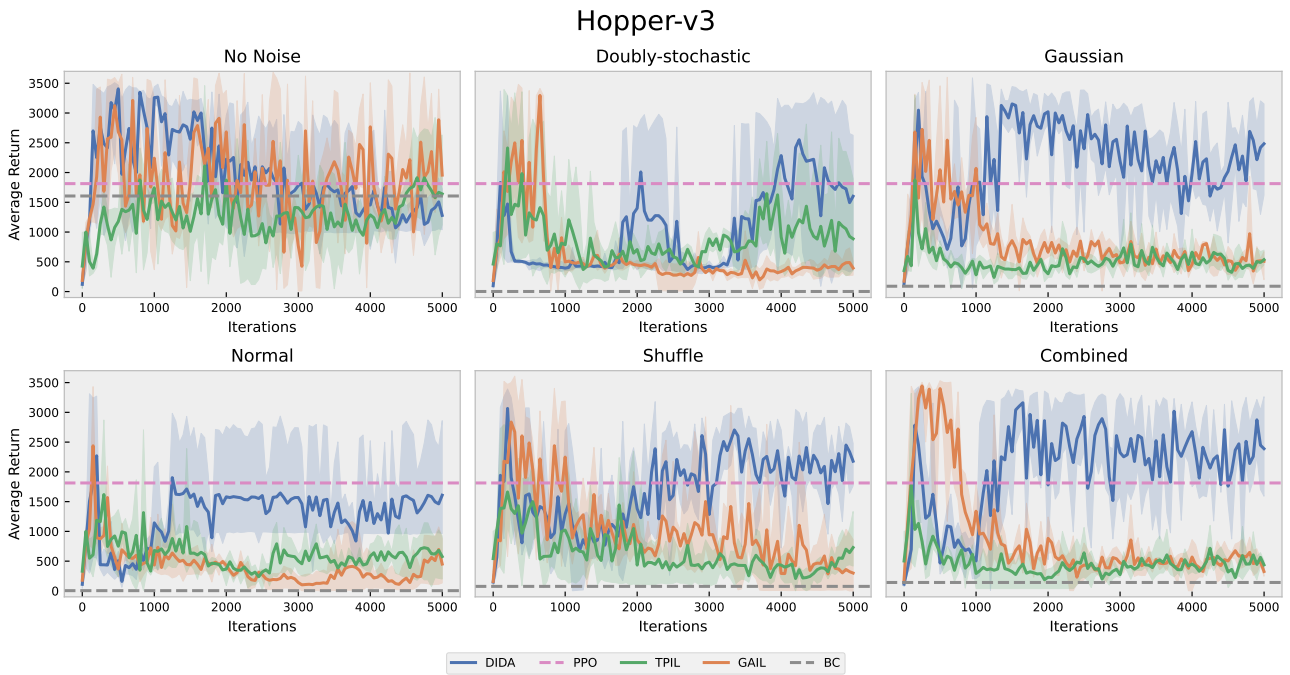


Figure 9. Performance curves of Section 6.1 on Hopper.

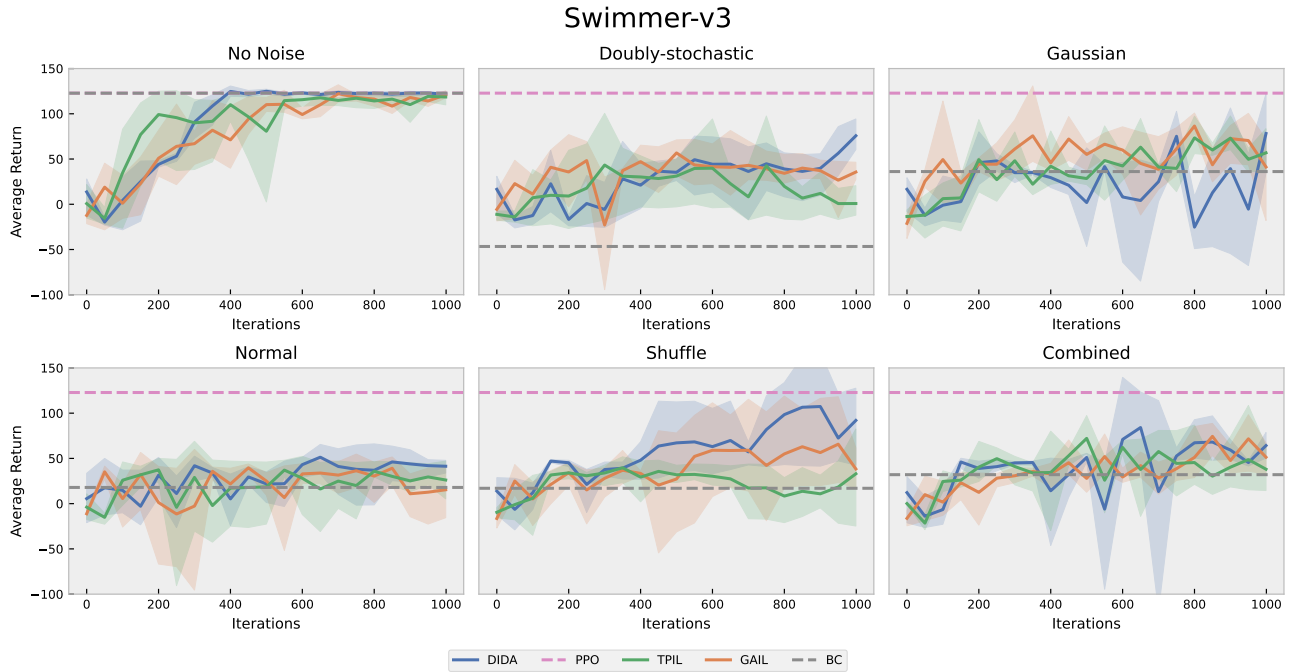


Figure 10. Performance curves of Section 6.1 on Swimmer.

We plot the performance curves of DIDA, TPIL, and GAIL over time, with the hopper environment in Figure 1 and the swimmer environment in Figure 2. The pink dotted line represents the return of the expert policy trained with PPO, and the gray dotted line shows the performance of BC. The SAIL curve is not included in the figure because its performance is too poor to be plotted on the same figure with other methods.

C.2. The full performance figures of Figure 7

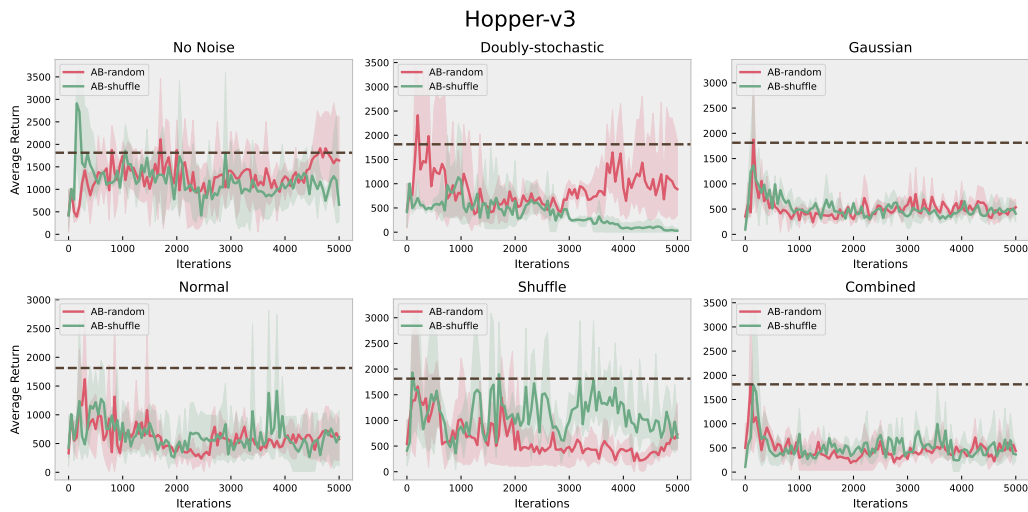


Figure 11. Performance comparison of TPIL methods with anchor-buffer-random and anchor-buffer-shuffle on multiple noisy datasets in the Hopper environment.

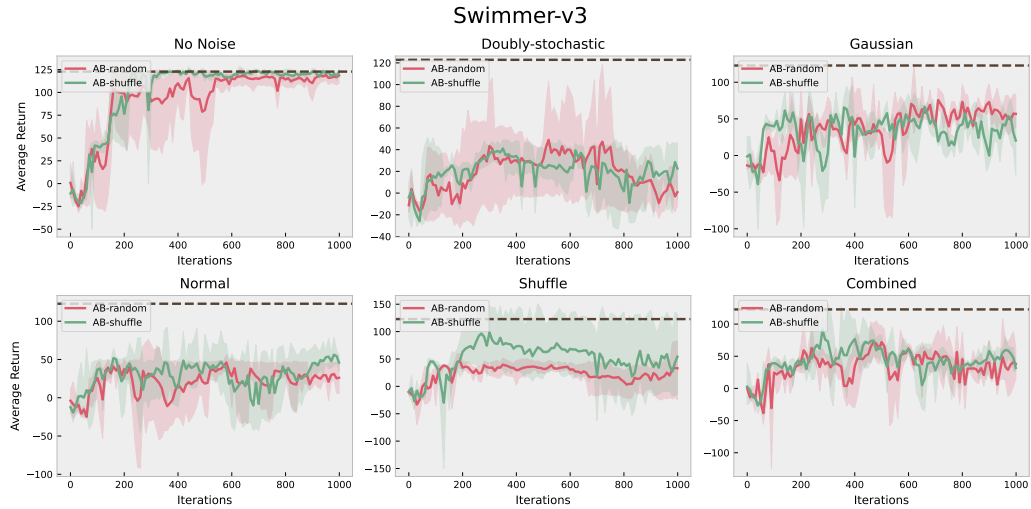


Figure 12. Performance comparison of TPIL methods with anchor-buffer-random and anchor-buffer-shuffle on multiple noisy datasets in the Swimmer environment.

We evaluated the performance difference of anchor-buffer-random and anchor-buffer-shuffle on multiple noisy datasets in the Hopper and Swimmer environments, with TPIL as the baseline method. As shown in Figure 11 and Figure 12, the two anchor buffer generation methods do not have a significant impact on performance. In most tasks, anchor-buffer-random performs slightly better than anchor-buffer-shuffle with smaller variance, because anchor-buffer-random obtains the ideal anchor dataset; while anchor-buffer-shuffle tries to imitate the outputs of anchor-buffer-random. However, as mentioned in Section 6.2, anchor-buffer-shuffle is more reasonable and practical, and our method DIDA with anchor-buffer-shuffle eventually achieves better performance than other baseline methods, which further demonstrates the superiority of DIDA.

C.3. Rendered trajectories

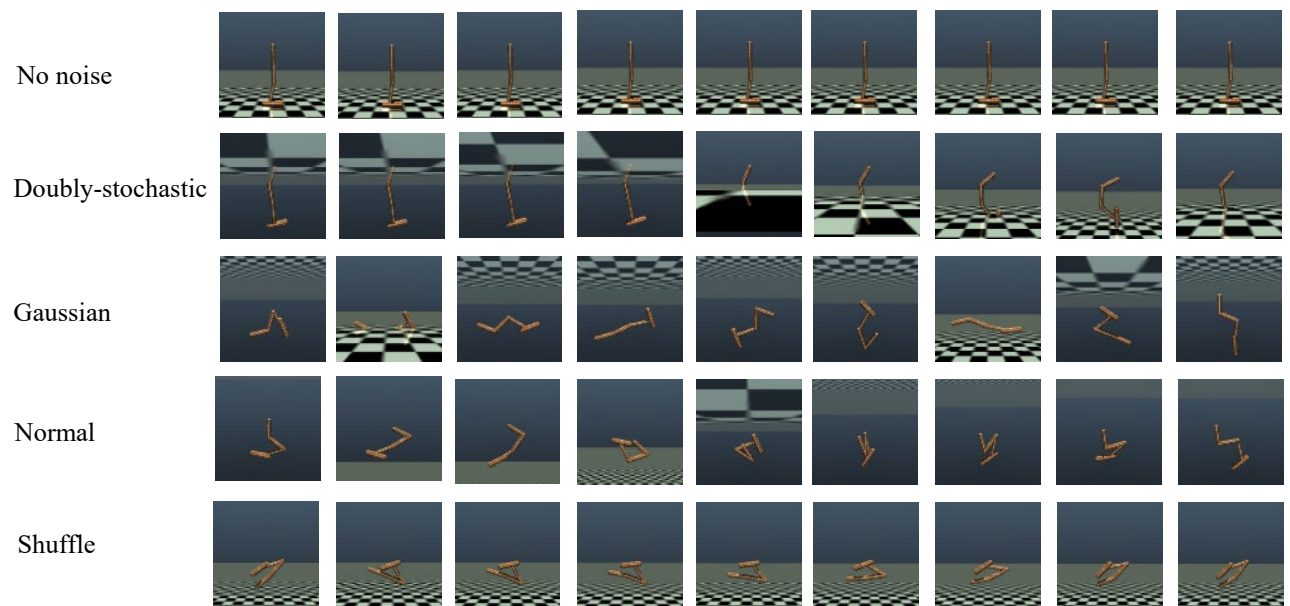


Figure 13. The rendered trajectories from five types of noisy states.

C.4. The t-SNE plots on latent embeddings of Figure 4

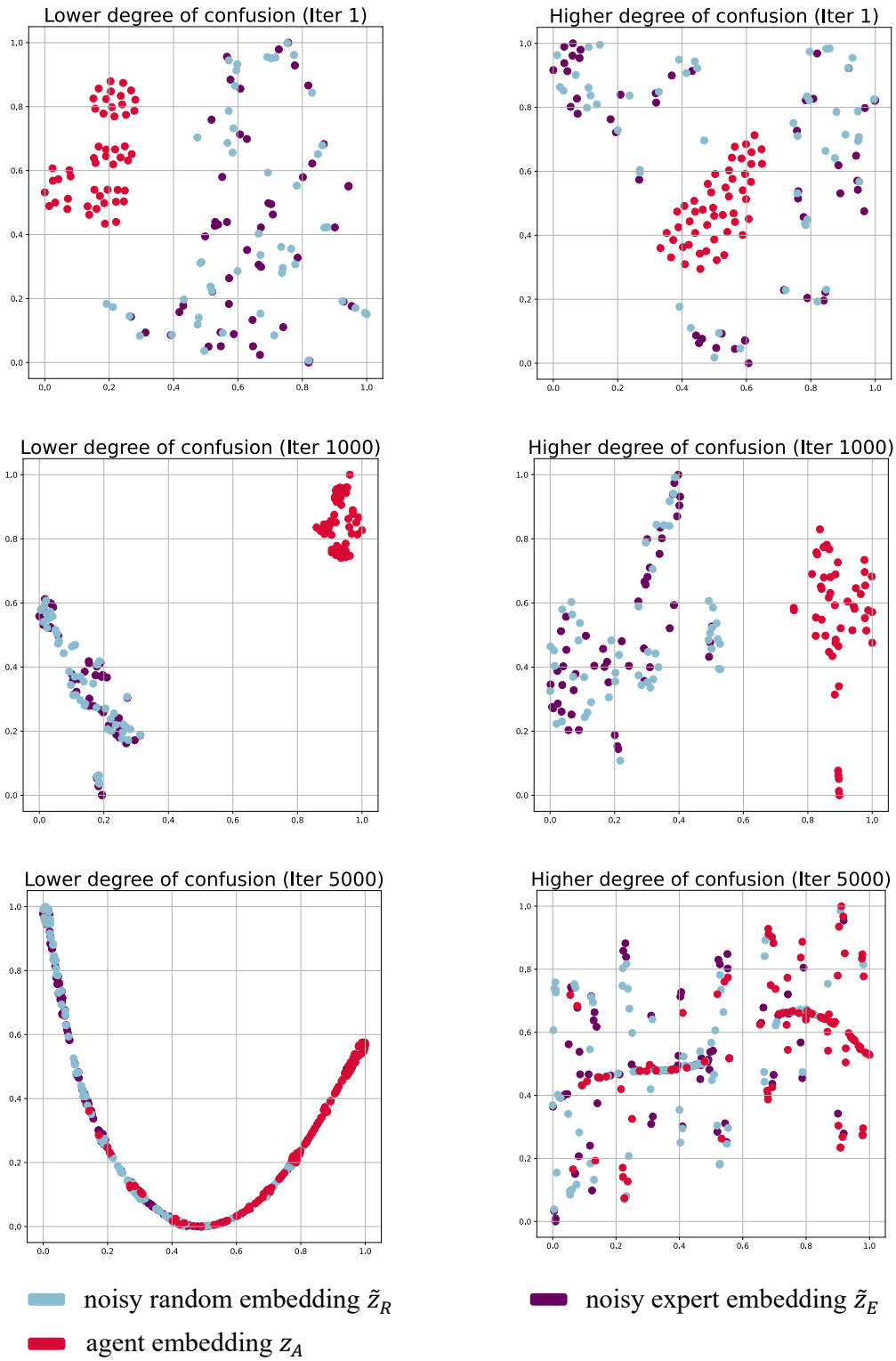


Figure 14. The t-SNE plots on latent embeddings of iter-1, iter-1000 and iter-5000, corresponding to the three rows from top to bottom. For each row, the two t-SNE plots corresponding to sample's embedding in Z_A , \tilde{Z}_R , and \tilde{Z}_E . The left plot corresponds to the 100 samples with the smallest degree of confusion while the right one corresponds to the 100 samples with the largest degree of confusion.

The first row of Figure 14 shows the results of the untrained model. The two clusters are close to each other because the randomly initialized feature encoder cannot extract embeddings that strongly correlated with the categories. The noise discriminator will likely classify data from the three different datasets into the same category. The second row of Figure 14 shows the results of the model after training for 1000 iterations. The clusters in the left and right figures are far apart, indicating that the embeddings at this time contain plenty of domain information. The third row of Figure 14 shows the results of the model after training for 5000 iterations. Most of the domain information in the embeddings has been eliminated at this time, and the points from different datasets in the t-SNE plot are mixed together and difficult to distinguish.

C.5. The full t-SNE plot on embeddings of different noise

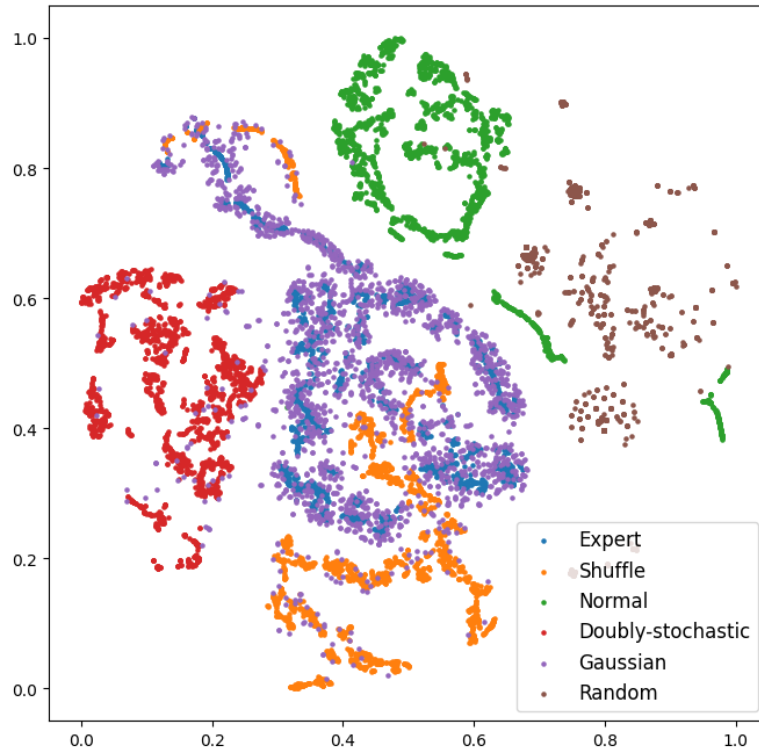


Figure 15. The t-SNE plot of the states from the random policy dataset, the expert policy dataset, as well as various noisy datasets. Different colors represent different categories. We can observe the characteristics of different noise, e.g., Gaussian noise is concentrated around the expert data, and random noise is the most dispersed. The distance between points in the t-SNE plot reflects the similarity of the data distributions.

D. Implementation Details

D.1. Detailed Description about Baselines

BC Behavior cloning is a type of imitation learning that aims to learn a policy by observing the behavior of an expert. Specifically, it learns a mapping from states to actions from expert demonstration data. This mapping can be a supervised learning model, such as a regression or classification model, or a reinforcement learning model.

PPO (Schulman et al., 2017) Proximal policy optimization (PPO) combines the benefits of trust region policy optimization (TRPO) with simpler implementation, better sample complexity, and improved performance in benchmark tasks. It proposes a novel objective function that allows for multiple epochs of minibatch updates, resulting in better optimization. PPO is tested on various tasks, including simulated robotic locomotion and Atari game playing, and outperforms other online policy gradient methods. The algorithm strikes a favorable balance between sample complexity, simplicity, and wall-time.

GWIL (Fickinger et al., 2021) Gromov-Wasserstein Imitation Learning (GWIL) is designed for cross-domain imitation

learning and it utilizes the Gromov-Wasserstein distance to align and compare states between the different spaces of the expert and imitation agents. By minimizing the Gromov-Wasserstein distance, GWIL aims to find an optimal coupling between the states of the expert and imitation agents. GWIL has been demonstrated to be effective in non-trivial continuous control domains, ranging from simple rigid transformations to arbitrary transformations of the state-action space.

SAIL (Liu et al., 2019) SAIL focuses on state alignment-based imitation learning, where the imitator and the expert have different dynamics models, and it aims to train the imitator to follow the state sequences in expert demonstrations as closely as possible. The state alignment is achieved by combining both local and global perspectives, which are integrated into a reinforcement learning framework using a regularized policy update objective. The methodology of SAIL also involves maximizing the curriculum reward, which is equivalent to optimizing the state visitation distributions for the Wasserstein distance. It’s worth mentioning that the official code that the authors of SAIL open-sourced is still under pre-release version, so the official implementation may not match the reported performance in the original paper. We run 3 seeds for each designed task and report SAIL’s best performance.

GAIL (Ho & Ermon, 2016) This work proposes a new general framework called GAIL for directly extracting a policy from data, as if it were obtained by reinforcement learning following inverse reinforcement learning. The framework draws an analogy between imitation learning and generative adversarial networks (GANs). This work derives a model-free imitation learning algorithm from this framework, which shows significant performance gains over existing model-free methods in imitating complex behaviors in large, high-dimensional environments. The methodology of GAIL involves recovering the expert’s cost function with inverse reinforcement learning and then extracting a policy from that cost function with reinforcement learning.

TPIL (Stadie et al., 2017) This work presents a method for unsupervised third-person imitation learning (TPIL), where an agent is trained to achieve a goal by observing a demonstration from a different viewpoint. The agent receives only third-person demonstrations and does not have correspondence between teacher and student states. The primary insight of the method is to utilize domain-agnostic features obtained from recent advances in domain confusion during the training process. TPIL aims to minimize class loss while maximizing domain confusion. It addresses questions regarding the algorithm’s sensitivity to hyper-parameter selection, changes in camera angle, and its performance compared to baselines. It also investigates whether the algorithm benefits from both domain confusion and velocity.

E. Hyper-parameters

Hyperparameter	Value
Policy hidden dim	(128, 128)
Value hidden dim	(128, 128)
Discriminator hidden dim	(128, 128)
Embedding size	10 Hopper, 7 Swimmer
batch size	2048
Optimizer	Adam
Learning rate	chooses from $[3 \times 10^{-4}, 1 \times 10^{-4}, 8 \times 10^{-5}, 6 \times 10^{-5}]$
Lambda	chooses from $[0.2, 0.5]$
Frequency of update	1 for encoder and policy discriminator 5, 7 for Hopper and Swimmer noise discriminator respectively
Agent rate clip	$[0.01, 0.99]$
Confuse prob clip	$[0.1, 0.9]$

Table 2. Hyperparameters of DIDA for all experiments.